Journal of Biomedical Optics 11(3), 034017 (May/June 2006)

Comparing the quantification of Förster resonance energy transfer measurement accuracies based on intensity, spectral, and lifetime imaging

Serge Pelet
Michael J. R. Previte
Massachusetts Institute of Technology
Department of Mechanical Engineering
77 Massachusetts Avenue, NE47-220
Cambridge, Massachusetts 02139

Peter T. C. So
Massachusetts Institute of Technology
Department of Mechanical Engineering and Division of Biological Engineering
77 Massachusetts Avenue, NE47-279
Cambridge, Massachusetts 02139

Abstract. The measurement of Förster resonance energy transfer (FRET) in microscopes can be realized by different imaging modalities. In the present work, reference FRET constructs are developed to allow the comparison of FRET microscopy measurements using intensity, spectral, and lifetime imaging. Complimentary DNA strands are respectively labeled with Oregon Green 488 (OG488) or tetramethylrhodamine (TMR). The OG488 dye is fixed at the 5′ end of one strand, and the TMR label position is allowed to vary along the complimentary strand. Since OG488 and TMR are FRET pairs, the FRET efficiency can be determined theoretically from the distance separating the two dyes of the double-stranded DNA molecules. Microscopic images are formed by imaging microcapillaries containing various mixtures of oligonucleotides labeled with the FRET fluorophore pair, only the donor, or only acceptor. Traditional two-channel intensity measurements are compared with spectrally resolved imaging and fluorescence lifetime imaging by calculating a FRET index. The latter proves to be the best method to quantify FRET efficiency in the image. More importantly, the intensity fraction of molecules undergoing FRET can be quantitatively measured in each pixel of the image. [DOI: 10.1117/1.2203664]

Keywords: Förster resonance energy transfer; fluorescence lifetime imaging; spectral imaging; two-photon microscopy.

Paper 05332R received Nov. 7, 2005; revised manuscript received Feb. 22, 2006; accepted for publication Feb. 22, 2006; published online May 23, 2006.

1 Introduction

Förster resonance energy transfer (FRET) is a process that takes places between two fluorophores interacting at short distances, resulting in a modification of their fluorescence intensity. The donor fluorophore transfers its electronic excitation energy via dipole-dipole interaction to the acceptor fluorophore. This leads to a quenching of the donor emission and an increase in acceptor emission, also called sensitized emission.

This phenomenon has been widely used in biology, such as in immunology to monitor molecular binding with immunofluorescence assays.[1–3] In this type of experiment, a binary response is expected from the assay; the presence of a FRET signal indicates the presence of the analyte in the solution. FRET is also extensively employed in single-molecule experiments to measure intramolecular distances and to follow protein conformational changes.[4,5] The relative changes in FRET efficiency can facilitate the mapping of protein folding pathways or the mechano-chemical transduction dynamics of motor proteins. However, applying FRET techniques to study protein interactions in living cells is challenging.[6–9] In this case, the presence of FRET will indicate that two proteins of interest interact intracellularly. However, it is often also desirable to quantify precisely the fraction of labeled protein that is engaged in binding interaction and the molecular distance of these protein pairs.

These quantitative experiments have gained in popularity with the discovery of the green fluorescent protein (GFP) and the generation of a whole set of similar fluorescent proteins (FPs), whose emission spectra cover the entire visible spectrum.[10–13] In a typical experiment to probe protein-protein interaction, a cell is modified to express two proteins of interest linked by a small peptide chain to a specific variant of the FP (Cyan FP and Yellow FP or GFP and dsRed are the most common FRET pairs).[14–17] Physical and biological processes, such as protein interaction, that bring the two FPs into close proximity, will result in energy transfer. The measurement of the fluorescence of these two proteins in each pixel of the image allows the amount of FRET occurring in each location of the cell to be quantified.

Jares-Erijman and Jovin[6] have presented an overview of the methods suggested and implemented to measure FRET *in vivo*. The most common ones are based on intensity measurements, but they are hampered with experimental artifacts due to cross-excitation and detection of the two fluorescent molecules. Many correction algorithms have been published and recover the FRET efficiency with good success, but they re-

---

Address all correspondence to Serge Pelet, ETHZ Hönggerberg, Institute for Biochemistry, HPM D8.2, CH-8093 Zürich; E-mail: serge.pelet@bc.biol.ethz.ch.

1083-3668/2006/11(3)/034017/11/$22.00 © 2006 SPIE

quire multiple sets of images with varying excitation and detection conditions, as well as with reference samples that contain only one of the fluorophore.[18–22] Acceptor photobleaching is an alternative method that avoids these complex correction schemes. With this process, the acceptor is photobleached and the donor intensity is compared before and after the photobleaching step to recover the FRET efficiency.[7,23] However, this technique is destructive and prevents repeated measurements on the same cell. Finally, fluorescence lifetime imaging is becoming more commonly used to quantify FRET. The quenching of the donor dye by the energy transfer process leads to a faster decay of the excited state that can be characterized in a microscope with picosecond temporal resolution.[14,24–27] The simple quantification of the reduction of the mean lifetime of the donor decay provides a relative measurement of the amount of FRET in the sample. With a careful analysis of the lifetime data with a biexponential model, all FRET parameters can be recovered completely (i.e., efficiency of the energy transfer, interaction distance between the two dyes, and ratio of donor involved in an energy transfer complex). This information is not available with any other intensity-based FRET measurements.

Using two-photon microscopy, we have studied the ability of intensity, spectral, and lifetime imaging modalities to recover FRET with well-characterized samples. This FRET construct was built based on dye-labeled DNA strands. By annealing complementary strands, we created a reference specimen with well-controlled energy transfer efficiency from the donor to the acceptor based on the fluorophore distance and spectral overlap. While FRET recovery using intensity, spectral, and lifetime imaging modalities has been studied previously, there is no quantitative comparison of the accuracy and precision of the three detection modalities in FRET recovery using the same reference specimen under an identical optical microscope, acquiring equivalent number of photons.

2 Theory

Energy transfer occurs when a fluorophore is promoted to its excited state in the presence of a second nearby fluorophore. The coupling of the transition dipole of these fluorophores results in the de-excitation of the donor and excitation of the acceptor. Due to the nature of this interaction, Förster predicted a dependence of the FRET efficiency on the sixth power of distance. Stryer and Haugland demonstrated this experimentally with linear polypeptides of varying lengths.[28] The efficiency E of the process varies as function of the distance R between the two molecules as:

$$E = \frac{R_0^6}{R_0^6 + R^6}, \tag{1}$$

where R_0 is called the Förster distance and corresponds to the separation were 50% of the donor fluorescence is converted into the energy transfer process. This parameter depends on the index of refraction of the medium n, the quantum yield of the donor molecule Q_D, the orientation factor κ, and the overlap integral J.

$$R_0^6 = \frac{9000 \ln(10) \kappa^2 Q_D}{128 \pi^5 N_A n^4} J. \tag{2}$$

κ represents the relative orientation of the transition dipole of the donor and acceptor molecules. In most cases, a random interaction is assumed, and this factor is set to $2/3$. The overlap integral J represents the energy overlap between the emission of the donor and the absorption of the acceptor. For well-matched fluorophore pairs, R_0 is on the order of 50 to 60 Å.[29,30] The efficiency of the energy transfer process (E) can be linked to physically measurable parameters, such as the fluorescence intensity of the donor I or its fluorescence lifetime τ.

$$E = 1 - \frac{I_F}{I_D} = 1 - \frac{\tau_F}{\tau_D}, \tag{3}$$

where the subscript D represents a sample with only the donor present, and the subscript F is a FRET sample, where both donor and acceptor are present.

To measure FRET in a living cell under a microscope based on steady-state intensity measurements, a series of images are recorded: a FRET sample and reference samples containing only the donor or the acceptor fluorophore under various imaging conditions. A three character symbol will be used to refer to each type of image: ${}^{2}_{1}X$. X refers to the sample studied: F for sample with FRET, A for a sample with only acceptor fluorophores, and D for a sample with donor alone. The subscript 1 refers to how the sample is excited (either a for excitation in the acceptor spectrum or d for excitation in the donor excitation spectrum). The superscript 2 refers to the emission light that is detected (a for detecting in the acceptor emission spectrum, d for detecting in the donor emission spectrum, or s for spectrally resolved detection). Furthermore, for the purpose of the correction algorithm, it is necessary to differentiate the contributions of the donor or acceptor to an image. Therefore, the three character symbol representing the image can be complemented by a lower letter a or d to refer only to the contribution of the acceptor or donor to the signal. A bar over the symbol indicates the theoretical signal expected if no FRET was present in the sample. As an example, $\overline{{}^{a}_{d}Fd}$ refers to an image of a FRET sample excited at the donor wavelength, detected in the acceptor channel, and considering only the contribution of the donor in the case where no FRET was present.

2.1 *Two-Channel Measurements*

FRET is characterized by a decrease in donor intensity and an increase in acceptor intensity. For cellular systems, a single image (${}^{d}_{d}F$) measurement of the donor emission does not allow an accurate quantification of FRET, because it is not possible to separate intensity changes due to intracellular concentration variation change or an energy transfer processes. Thus, two images of the donor (${}^{d}_{d}F$) and acceptor (${}^{a}_{d}F$) emission need to be recorded to establish that the ratio of acceptor-over-donor emission has increased. Many artifacts influence this ratio. Most importantly, the direct excitation of the acceptor at the donor wavelength can lead to an increase in the acceptor channel unrelated to any FRET process. Thus, a third image (${}^{a}_{a}F$) is recorded under excitation at the acceptor wavelength to quantify the acceptor concentration, and to correct for its contribution. The recovery of the FRET index can be further improved by calibration of the spectral bleed-through and cross-excitation of both fluorophores. Calibration is performed by measuring these three aforementioned images using reference samples that contain either the donor or the acceptor. A total of nine images are thus required to calculate the fully corrected FRET image: three images from the sample itself and six (three from each) from the donor and acceptors alone.

Many algorithms have been developed to retrieve the amount of FRET present in the sample. Berney and Danuser published a comparison of the most common methods, and concluded that the algorithm published by Gordon et al. provides the best recovery of the FRET parameters hidden in the image.[18,19] This algorithm compensates for the common artifacts found in FRET experiments such as spectral bleed-through and cross-excitation. It allows the FRET1 index to be calculated, which is the loss of donor signal due to FRET:

$$\mathrm{FRET1}=\frac{{}^{a}_{d}F-{}^{d}_{d}F\dfrac{{}^{a}_{d}D}{{}^{d}_{d}D}-\overline{{}^{a}_{a}Fa}\left(\dfrac{{}^{a}_{d}A}{{}^{a}_{a}A}-\dfrac{{}^{a}_{d}D}{{}^{d}_{d}D}\dfrac{{}^{d}_{d}A}{{}^{a}_{a}A}\right)}{G\left(1-\dfrac{{}^{d}_{d}A}{{}^{a}_{d}A}\dfrac{{}^{a}_{d}D}{{}^{d}_{d}D}\right)},$$

where

$$\overline{{}^{a}_{a}Fa}=\frac{{}^{a}_{a}F-{}^{a}_{d}F\dfrac{{}^{a}_{a}D}{{}^{a}_{d}D}}{1-\dfrac{{}^{a}_{d}A}{{}^{a}_{a}A}\dfrac{{}^{a}_{a}D}{{}^{a}_{d}D}},$$

and

$$G=\frac{QY_a}{QY_d}\frac{\phi_a}{\phi_d}\frac{T_F}{T_D}. \tag{4}$$

G is a dimensionless factor that scales the acceptor signal intensity to the donor intensity. QY is the quantum yields of the dye, ϕ is the fraction of fluorescence transmitted through the filter set and measured by the detector, and T represents the fractional transmission of neutral density filters.

FRET1 is related to the theoretical FRET efficiency, but it still depends on the donor emission intensity. To correct for that, a FRET2 index, which is the ratio of FRET1 over the total amount of donor emission if no FRET was present ($\overline{{}^{d}_{d}Fd}$), is introduced and varies theoretically between 0 and 1.

$$\mathrm{FRET2}=\frac{\mathrm{FRET1}}{\overline{{}^{d}_{d}Fd}},$$

where

$$\overline{{}^{d}_{d}Fd}={}^{d}_{d}F+\mathrm{FRET1}\left(1-G\frac{{}^{d}_{d}A}{{}^{a}_{a}A}\right)-\overline{{}^{a}_{a}Fa}\frac{{}^{d}_{d}A}{{}^{a}_{a}A}. \tag{5}$$

To obtain these corrected images (FRET1 and FRET2), three images of three samples (FRET, donor, and acceptor samples) must be collected with two detection channels and two different excitation wavelengths. The reference sample images are always present in the algorithm as a ratio between two reference images, thus the average of this value for the entire image can be used in the algorithm to minimize the error.

2.2 *Spectral Imaging*

The whole emission spectrum of the sample in each pixel of the image can be measured with spectrally resolved microscopy.[31–33] At each pixel, the spectral information can be represented as a 1-D vector ${}^{s}_{d}F(i)$, where i is an index of the spectral channel. This supplementary information can be used in two different ways. The simplest method is to divide the full spectral range into two parts, whose sums provide the donor and acceptor images.

$${}^{d}_{d}F=\sum_{i=j}^{k}{}^{s}_{d}F(i)\text{ and }{}^{a}_{d}F=\sum_{i=m}^{n}{}^{s}_{d}F(i), \tag{6}$$

where j, k, m, and n are the limits for the integration of the spectrum. The images calculated can be fed into the Gordon algorithm to calculate the FRET index. This technique provides the advantage of selecting the most suitable spectral window for both emitters after the acquisition has been done. The second method calculates for each pixel of the image the contribution of the donor and acceptor species based on their known spectra (spD and spA, represented by a single row vector) obtained from the reference samples. The spectral information at each pixel is a linear superposition of the spectrum of the donor and the acceptor.

$${}^{s}_{d}F(i)={}^{d}_{d}F\cdot\mathrm{sp}D(i)+{}^{a}_{d}F\cdot\mathrm{sp}A(i). \tag{7}$$

The images ${}^{d}_{d}F$ and ${}^{a}_{d}F$ are obtained by a least-square optimization. This spectral decomposition method has the advantage of removing all the emission bleed-through, and it results in a simplified version of the Gordon's algorithm.

$$\mathrm{FRET1}=\frac{{}^{a}_{d}F-{}^{a}_{a}F\dfrac{{}^{a}_{d}A}{{}^{a}_{a}A}}{G\left(1-\dfrac{{}^{a}_{d}A}{{}^{a}_{a}A}\dfrac{{}^{d}_{a}D}{{}^{d}_{d}D}\right)},$$

and

$$\mathrm{FRET2}=\frac{\mathrm{FRET1}}{{}^{d}_{d}F+\mathrm{FRET1}}. \tag{8}$$

The terms that correct for the emission bleed-through, such as ${}^{a}_{d}D/{}^{d}_{d}D$, equal zero and only the cross-excitation ratios remain in the algorithm. Note that a new term ${}^{d}_{a}D/{}^{d}_{d}D$ is present to replace the ${}^{a}_{a}D/{}^{a}_{d}D$ ratio that accounts for the excitation of the donor under acceptor illumination. The spectrally resolved measurements require the recording of an image set consisting of typically 16 frames with roughly 10-nm bandwidth. This type of image set can be obtained in a single acquisition with a laser scanning microscope and a spectrally resolved detection, or using a filter wheel and a charge-coupled device (CCD) detector in wide-field imaging systems. In both cases, two different excitation wavelengths for each of the three samples (a total of six image sets) are required to obtain

FRET2. Practically, FRET measurements in a spectral imaging microscope can be implemented as easily as traditional two-channel detection. For apparatuses that require independent recording of the various spectral components, image set collection times will increase.

2.3 *Lifetime Imaging*

The quenching of the donor fluorescence by the energy transfer process leads to an acceleration of the dynamics of the donor excited state, i.e., a shortening of its lifetime. The chromophore engaged in a FRET complex will have a characteristic lifetime τ_F fixed by the geometry of the protein-protein interaction. In the case where both free and bound proteins are present in the sample, the fluorescence lifetime will be a double exponential decay with the time constants of the free and fretting dye. The contribution of each population to the lifetime relaxation is proportional to their respective concentration in the sample.

The analysis of a fluorescence lifetime imaging microscopy (FLIM) is best realized with a global fitting algorithm.[34,35] Equation (9) is a two-exponential global fitting model that assumes the existence of two fluorophore populations with two lifetimes τ_F and τ_D [corresponding to the coefficients c_1 and c_2 in Eq. (9)], which are optimized for the whole image. The initial intensity c_{2i+1} and the intensity ratio of the two lifetime components c_{2i+2} at each pixel i vary spatially. Note that c_{2i+2} is bound between 0 and 1 to prevent negative contributions from the two exponentials. IR is the instrument response of the system, which is convolved with the expected fluorescence decay to obtain the measured intensity decay.

$$I_i^{\mathrm{model}}(t) = \int_0^t \mathrm{IR}(t-T)\cdot c_{2i+1}\left[c_{2i+2}\exp\left(-\frac{T}{c_1}\right) + (1-c_{2i+2})\exp\left(-\frac{T}{c_2}\right)\right]dT. \qquad (9)$$

The lifetime analysis of the FRET sample provides the exact ratio of interacting protein in each location of the sample. Furthermore, using Eqs. (1) and (3), it is possible to calculate the efficiency of the FRET process and obtain an approximate measurement of the distance separating the donor from the acceptor. A similar quantification cannot be realized with intensity-based measurements.

To compare these measurements with the intensity and spectral results, it is possible to convert the results from the global fitting algorithm to extract a FRET2 index. Assuming that only the donor emission is detected through the donor filter, FRET2 can be simply expressed as:

$$\mathrm{FRET2} = \frac{\overline{{}^{d}_{d}Fd} - {}^{d}_{d}F}{\overline{{}^{d}_{d}Fd}},$$

where

$${}^{d}_{d}F = \sum_t I_{\mathrm{data}}(t),$$

$$\overline{{}^{d}_{d}Fd} = \sum_t \left[\int_0^t G(t-T)\cdot c_{2i+1}\exp\left(-\frac{T}{\tau_D}\right)\right]. \qquad (10)$$

An intensity image corresponding to ${}^{d}_{d}F$ can be created from the sum over all time channels in the FLIM image. The image of the donor without the presence of FRET is easily calculated by setting the coefficient c_{2i+2} to zero, which represents a decay without contribution from the FRET species.

The practical advantage of the lifetime imaging technique is that only a single image from the FRET sample at the donor excitation and emission wavelengths is needed to extract the energy transfer parameters. In practice, a donor-only sample is also measured during the same experiment as a negative control.

3 Methods

The microscope setups for lifetime[34] and spectral imaging[36] have been previously published. Briefly, the two-photon microscope is based on a modified inverted microscope (Axiovert 110, Zeiss, Göttingen, Germany) using a femtosecond laser (Mira, Coherent, Santa Clara, California) as light source working in epi-fluorescence mode. For the two-channel image acquisition mode, the fluorescence is sent to the top port of the microscope, where it is split in a green and red detection channel using a dichroic mirror (Q565LP) and appropriate filters (green: HQ500LP and E530SP, Red: HQ610/75) from Chroma (Rockingham, Vermont) and detected by single-photon counting photomultiplier tubes (PMTs) (R7400P, Hamamatsu, Bridgewater, New Jersey). In lifetime imaging mode, the same optical path is used, and the signal from the green channel is sent to a time-correlated single-photon-counting (TCSPC) card (SPC-730, Becker-Hickl, Berlin, Germany). In the spectral imaging mode, the fluorescence is reflected out of the microscope and sent to an imaging spectrograph (MS125, Oriel, Stratford, Connecticut) with a 16-channel PMT (R5900U-00-L16, Hamamatsu, Bridgewater, New Jersey) positioned at the image focal plane.

30 base pair modified oligonucleotides were purchased from MWG Biothech Incorporated (High Point, North Carolina). The donor dye was Oregon Green 488 (OG488), which was inserted internally in the strand through a C6 linking arm attached to a thymine at position 11 or 21 on strand B (5′-TCA CAT ACA A**T**A CAA TAC AA**T** ACA ATA CGA-3′). Tetramethylrhodamine (TMR) was placed at the 5′ end of the complementary strand (5′-TCG TAT TGT ATT GTA TTG TAT TGT ATG TGA-3′). The labeling modifications are described in Tables 1 and 2. The oligos were diluted in TE buffer and heated at 95 °C for five minutes for annealing. The final concentration of the double stranded DNA solution was 2 μM.

Hanging-drop slides filled with DNA solution were imaged to record the fluorescence properties of the various samples. The images were acquired with 100 mW of excitation power (measured outside of the microscope, corresponding to approximately 20-mW power at the specimen) through a 40× objective (Fluar, 1.3 NA, Zeiss) at 760 nm for the donor images and 840 nm for the acceptor images. For each excitation wavelength, both donor and acceptor images are recorded simultaneously by the green and red detection channels. To form images containing multiples solutions, 50-μm capillar-

Table 1 Modification of the single-strand DNA by fluorescent dyes.

ss-Oligos	Strand	Modification
dna-A	A	—
dna-B	B	—
dna-TMR	A	TMR on 5′ end
dna-OG488-20	B	OG488 on T11
dna-OG488-10	B	OG488 on T21

ies (Vitrocell 8505, Vitrocom, Mountain Lakes, New Jersey) filled with solution and placed on a coverslip were imaged using a 25× objective (Plan-Neofluar, 0.8 NA, Zeiss) and 200 mW of power (measured outside of the microscope).

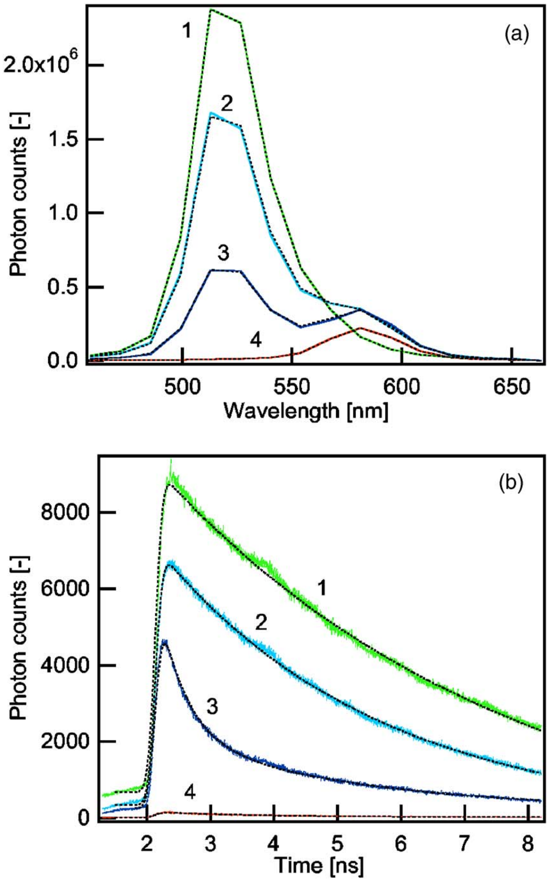

Fig. 1 (a) Bulk emission spectra and (b) lifetime from the double-stranded DNA measured in the microscope. 1. OG488-ds, 2. OG488-20-TMR, 3. OG488-10-TMR, 4. TMR-ds. The solid lines are the experimental data and the dotted lines correspond to the fits for each dataset.

4 Results

Figure 1 shows the emission spectra and fluorescence decay from the double-stranded DNA solutions. The linkage of the dyes to the DNA backbone slightly affects the photophysics of each compound. Oregon Green lifetime is extended to 4.55 ns (±0.02, $\chi_R^2=16.4$) compared to the 3.89 ns (±0.015, $\chi_R^2=2.95$) for a measurement of the same dye in water. Due to varying experimental conditions, it is difficult to absolutely compare these retrieved values with literature results, but as a relative reference, these results are within the range of those reported previously.[37] The lifetime of tetramethylrhodamine on DNA [1.63 ns (±0.03, $\chi_R^2=1.25$)] is, however, shorter than the dye alone in solution [2.32 ns (±0.01, $\chi_R^2=2.01$)], which again are within the range of previously reported literature values.[38] The evolution of the quenching of the donor emission where no acceptor is present, to an acceptor placed 20 and 10 base pairs away, is clearly visible in the spectral and lifetime measurements. The increase in sensitized emission can also be observed in the red part of the emission spectrum.

Using Eq. (3), it is possible to calculate the efficiency of the FRET process for the two different FRET constructs for three different imaging modalities. The theoretical efficiency expected for these constructs can be compared with a cylindrical model that is used to calculate the distances for similar molecules.[39] The Förster radius was calculated using Eq. (2) and was found to be 65 Å for the transfer from OG488 to TMR. The intensities with and without donor are calculated from the average of the first seven channels in the spectral image, and the uncertainty is obtained from the standard deviation across the image. The efficiency for spectrally resolved measurements is obtained by linear spectral decomposition of the spectra averaged across the image using normalized spectra from OG488-ds and TMR-ds. The uncertainty on the efficiency is calculated from the error obtained on the coefficients of the fits. The efficiency for the FLIM modality is obtained by fitting the data with a convolution between the instrument response and an exponential decay. Optimization with a single exponential decay delivers a good fitting curve for OG488-20-TMR, yielding a time constant of 3.1 ns (±0.01, $\chi_R^2=5.63$). To obtain a good fit for the OG488-10-TMR data, a double exponential decay is necessary. The faster time constant is 0.43 ns (±0.005) and represents 69% of the decay, and the slower time constant is 3.1 ns (±0.01, $\chi_R^2=3.01$). For the double exponential decay, only the fastest time constant is used to calculate the efficiency; however, there is a slight difference in lifetime between OG488-ds and OG488-10-TMR that we cannot explain definitively. One can see in Fig. 1(b) that some TMR signal leaks into the green channel. This signal will be increased when FRET is present. As TMR has a faster lifetime than OG488, it might lead to an apparent faster decay of the long lifetime. However, one does not expect this contribution to be very large, because the over-

Table 2 Composition of the double-stranded DNA.

ds-Oligos	Strand 1	Strand 2
OG488-ds	dna-A	dna-OG488-20
TMR-ds	dna-TMR	dna-B
OG488-20-TMR	dna-TMR	dna-OG488-20
OG488-10-TMR	dna-TMR	dna-OG488-10

Table 3 Comparison of the expected and measured efficiencies for the two DNA FRET constructs using different imaging modalities. The distances are obtained from a cylindrical model of DNA.

	OG488-10-TMR	OG488-20-TMR
r [Å]	46.5	75.8
E_{theory}	0.88	0.28
$E_{\text{intensity}}$	0.74±0.2	0.32±0.08
E_{spectral}	0.75±0.02	0.31±0.01
E_{lifetime}	0.90±0.01	0.32±0.005

all TMR signal will at most double in the FRET situation. The calculated FRET efficiencies for the various imaging modalities are summarized in Table 3.

To compare the three data acquisition techniques in a real imaging situation, an image was composed with three capillaries filled with different mixtures of the DNA constructs. Capillary A contains the OG488-ds and TMR-ds at a concentration of 1 μM, which should not display any FRET. Capillary C contains only the OG488-10-TMR double-stranded DNA at 1 μM, which is expected to exhibit strong FRET. Capillary B is filled with a 1:1 mixture of the solutions used for capillaries A and C. Figure 2 shows the intensity measured in the green and red channel under excitation at 760 nm. The decrease in green emission and increase in red counts from capillary A to C is clearly visible. Since the donor and acceptor concentrations are equal between the three solutions, the only reason for this intensity variation is the occurrence of FRET in the last two capillaries. Both the spectral images and the intensity datasets have been corrected for the flatness of the fluorescence field.

The maximum counts in the green channel under excitation at 760 nm are on the order of 3000 photons. This is the case for all three imaging modalities. For the spectral and two-channel data acquisition, 20 frames of 128×256 pixels with a 5-kHz pixel clock were added for a total acquisition time of 250 s. For the FLIM measurements, the acquisition time was slightly longer (300 s) for a roughly equivalent number of detected photons. Note, however, that for the two intensity measurements, a second dataset at the acceptor excitation wavelength has to be recorded, which doubles the true FRET acquisition time.

Figure 3 shows the average counts measured in each capillary for the three imaging modalities. Again, the intensity image clearly shows the decrease in donor emission and the increase in acceptor emission, respectively. The emission spectra show a large change in the green part of the spectrum, but the change in donor intensity is less noticeable. The averaged fluorescence decays also demonstrate the increase in quenching of the donor emission in capillary B and C versus A. Note that in the imaging mode, the memory buffer on the TCSPC card limits the size of the acquisition. For our image, only 64 temporal channels have been used, compared to the 4096 in the bulk measurements from Fig. 1, thereby limiting the sensitivity of the lifetime detection in an imaging situation.

The spectrally resolved data were analyzed using the FRET algorithms presented earlier. The reference images for the donor and acceptor were obtained from the OG488-ds and TMR-ds solution in hanging-drop slides under the same im-

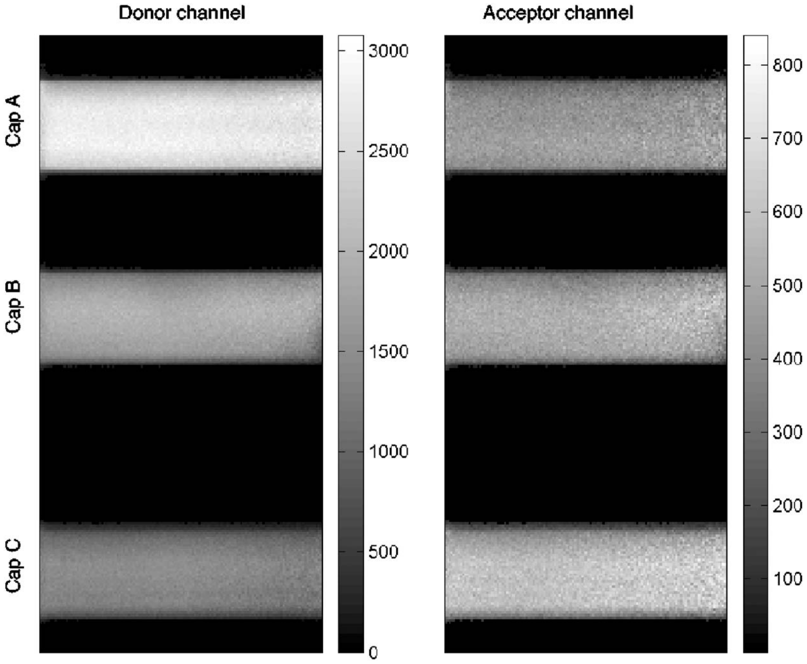

Fig. 2 Images of the three capillaries in the donor channel and acceptor channel under donor excitation (760 nm). Capillary A contains OG488-ds and TMR-ds at 1 μM (no FRET). Capillary C contains OG488-10-TMR (high FRET), and Capillary B a 1:1 mixture of the solutions used in capillaries A and C.

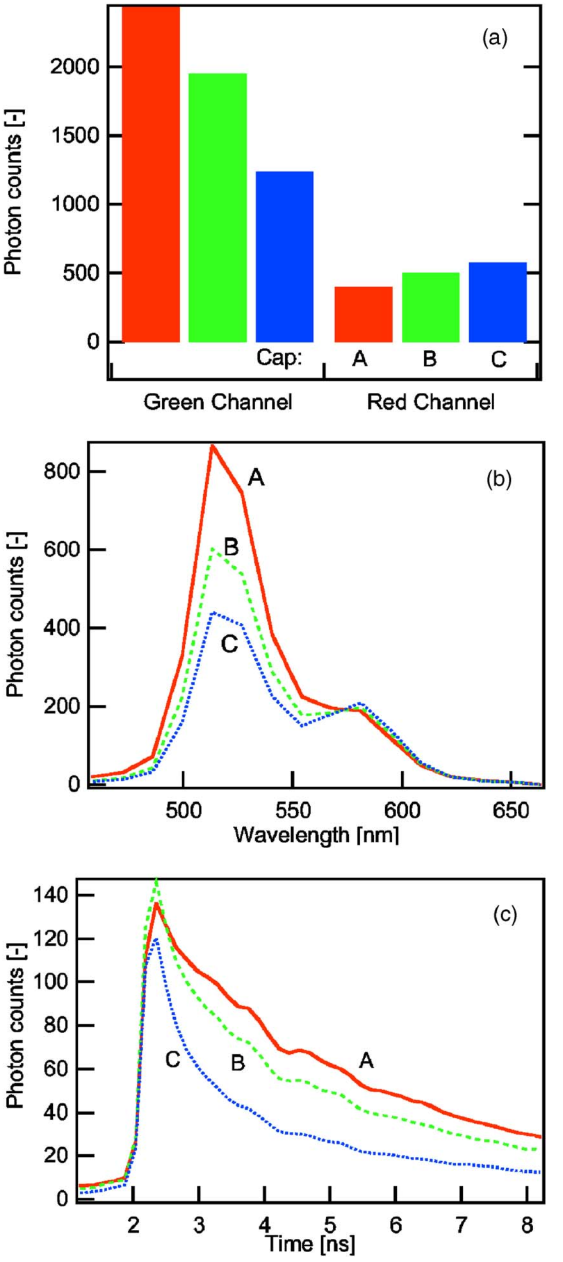

Fig. 3 Average photon counts in each capillary with the different imaging modalities for capillaries A, B, and C: (a) two-channel measurement, (b) spectral imaging, and (c) fluorescence lifetime microscopy.

aging conditions. The quantum yields for OG488 and TMR in solution are close to unity. However, the binding to the DNA modifies this, and TMR fluorescence is partially quenched by this interaction. Based on the lifetime measurements, a QY_a of 0.63 was calculated. The fractions of donor and acceptor emission measured with the two channel scheme were estimated using reference curves for the filters for the intensity measurements, and it is also used to account for the difference in sensitivity of the PMT in the green and red parts of the spectrum. For the spectral imaging, the sensitivity in the red is further reduced by the grating of the spectrometer, which is blazed at 400 nm. The transmission values T_F and T_D are equal to one, as no neutral density filter has been used. Overall, the G value for the two channel setup was found to be 19% for the two channel mode, 18% for the spectral imaging converted in two channel, and 21% for the spectral imaging with spectral decomposition. This means that for every five photons collected in the green channel, only one is measured in the red.

The FRET2 index was calculated for each pixel of the image using the four algorithms presented earlier. Figure 4(a) shows the average values and standard deviation calculated from each algorithm in the respective capillaries. For capillary A, the expected average should be zero; however, every algorithm delivers a slightly higher average FRET2 index. For each method tested, the FRET2 index increases almost linearly for capillary B and C. Figures 4(b) and 4(c) represent the histograms of the FRET2 retrieved in each capillary. The distributions retrieved with the lifetime algorithm are noticeably sharper than for the intensity-based methods.

The lifetimes can provide more information about the FRET construct present in the image. The global fitting algorithm was applied to a dataset formed by the image shown in Fig. 2, as well as a second FLIM image containing three capillaries, one (D) with no FRET similar to capillary A, and two containing mixtures (capillary E: 3:1 and capillary F: 7:1) of the solution used in capillaries A and C. The algorithm retrieved two lifetimes of 3.38 and 0.58 ns, and the ratio of fretting over total dye ($\chi_R^2=1.106$). The average values of the ratio as well as the histogram of the ratio are shown in Fig. 5. The expected ratio for capillaries A and D is, of course, zero. A ratio of one is expected for capillary C. However, as measured in the bulk solution, OG488-10-TMR exhibits a biphasic decay, and only 69% of the population relaxes with the fast time constant. Consequently, the ratio obtained by the global fit also reflects a lower fretting population. Finally, the standard deviations of FRET2 index measurements using these four approaches are shown in Fig. 6.

5 Discussion

The efficiencies calculated from all three modalities used for the measurement of the bulk DNA solutions are consistent with the expected efficiencies. In the present case, the bleedthrough of the acceptor in the green channel is reduced to a minimum. Therefore, the photon counts in this channel are directly proportional to the emission of the donor. These results are affected by one experimental artifact due to the presence of a nonFRETting donor. This can be caused either by unannealed donor strands or annealed donor strands with a complementary strand lacking the acceptor dye. This signal skews the efficiency calculation, and FRET efficiencies are lower than expected, especially at short distances where the quenching is important.

Only the lifetime measurements can distinguish between the FRETting and nonFRETting populations of the donor, because they exhibit different lifetimes. This phenomenon is predominantly seen in the OG488-10-TMR, where a double exponential decay is required to analyze the fluorescence decay properly. For the OG488-20-TMR sample, a double exponential can be used to fit the data. It does not provide any noticeable improvement of the fit, because the two time constants are very close and only a fraction of the decay (up to 6.5 ns) is acquired.

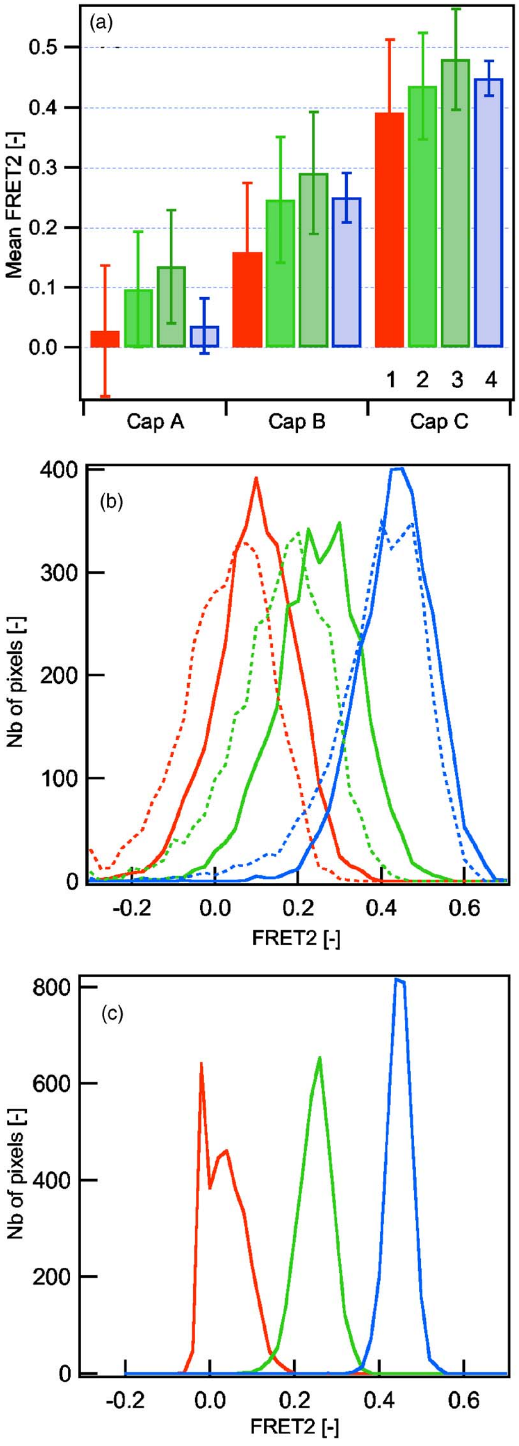

Fig. 4 (a) Mean FRET 2 indices retrieved in each capillary with different data analysis techniques. 1. Two-channel algorithm, 2. spectral imaging with spectral decomposition, 3. spectral imaging split for two channel algorithm, and 4. global fitting of FLIM data. (b) FRET 2 histogram for spectral imaging with decomposition (solid lines) and two-channel (dotted line) imaging in capillaries A, B, and C (in ascending order). (c) FRET 2 histogram for FLIM in capillaries A, B, and C.

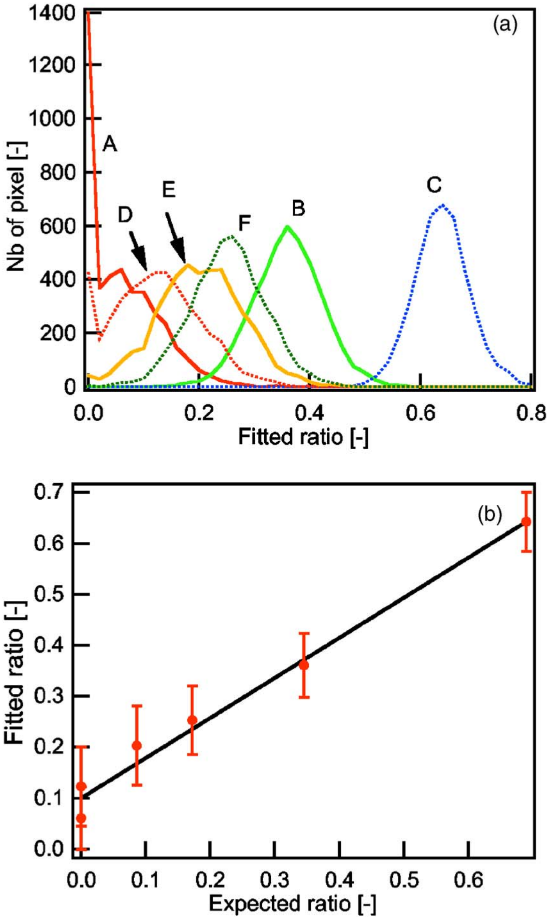

Fig. 5 (a) Ratio coefficients retrieved using the global fitting algorithm in six capillaries with various mixtures of OG488-ds and OG488-10-TMR (see text). The two lifetimes recovered are 3.38 and 0.58 ns. (b) Mean ratio coefficients obtained from the global fit plotted as function of the expected ratio coefficient. The solid line is a linear regression with a slope of 0.79 and offset of 0.1.

Doubly labeled DNA systems are used to quantify the accuracy and precision of intensity, spectral, lifetime FRET measurement approaches. While these DNA constructs do not recapitulate the complexity of measuring protein interactions in cells where FRET efficiency can be affected by environmental factors such as temperature and pH, the FRET efficiencies of these DNA constructs can be theoretically predicted and precisely controlled experimentally by varying the distance between the fluorophores. FRET has already been measured in many similar doubly labeled DNA systems.[39–43] A true comparison between all these studies is somewhat difficult, because the dyes and strands are not identical. However, the distances retrieved are comparable, which means that the overall energy process is not affected greatly by these slight dissimilarities. Therefore, the DNA construct is an excellent test system to evaluate the accuracy of these different imaging techniques to retrieve FRET in a microscopy image. As discussed in Thaler et al.[32] the development of FRET technology requires a set of well-quantified reference standard samples, against which the utility of different imaging technologies and probe pairs can be evaluated. We show that these doubly labeled DNA systems are very valuable in evaluating different FRET imaging modalities; we expect that they can also be used in the evaluation of different FRET fluorophore pairs and can quantify their Förster distances.

The use of the three capillaries allowed us to form an image containing different amounts of FRET in a well-controlled manner. This technique had one minor shortcoming. Due to the relatively large size of these capillaries (100-μm external dimension), the scanning area has to be large. To collect the largest fraction of emitted photons, an objective with a large NA is needed. The 25× objective chosen for these experiments is a good compromise between high NA (0.8) and low magnification. It was still necessary to scan the laser beam at large angles to cover a distance of more than 250 μm. As a result, the collection efficiency in the periphery of the image is decreased by a factor of 4. This artifact is accounted for by using a reference image from a fluorescent solution with the same scanning parameters. Figure 2 shows that this correction is effective, because the intensity throughout the capillaries is relatively uniform. However, the photon counting noise is increased by that procedure. The distribution of the photon counts is expected to obey Poisson statistics, but the standard deviations for each capillary in the images are roughly 10 to 20% larger than the square root of the mean.

The standard deviation for FRET2 due only to Poisson noise is only marginally smaller than the measured FRET2 standard deviation. Therefore, this distribution in FRET2 indices is due to the intrinsic noise of the measurement and is not introduced by experimental artifacts. Improvement in the FRET2 signal could be obtained by increasing the acquisition time or the detected photon flux.

The results obtained here are clearly dependent on the experimental conditions and instrument used. We are fortunate to have a single instrument that combines three different types of imaging techniques and therefore allows an accurate comparison of these modalities. Other setups dedicated to one of these imaging techniques might be more sensitive than our microscope. However, we try to draw some general conclusions on the implications of our results for *in vivo* FRET imaging.

The FRET2 index calculated is very sensitive to the value of the G variable. Because we used different detection schemes, we had to determine its value with precision. However, for most users working on a single instrument with a given FRET pair, an inaccurate G value will not prevent a relative comparison of the measured FRET2 indices. A precise quantification of G will be necessary only if different setups are used, or in cases where the quantum yields of the dyes are dependent on the experimental conditions. Other algorithms use different correction normalization factors, which can be more readily available than quantum yields, such as the respective absorbance of the acceptor and the donnor. Recent studies from Hoppe, Christensen, and Swanson, and Bonamy, Guiochon-Mantel, and Allison, allow to recover stoichiometry of FRET interactions, but require the measurement of a reference FRET construct, which is not always available for *in vivo* experiments.[21,44]

For intensity-based techniques, the error in the FRET2 index determination is only marginally dependent on calibration factors such as G and bleed-through calibrations (which can be obtained from a large number of reference samples), but mostly arises from the addition of multiple images, each having an intrinsic noise. Moreover, the algorithm relies mostly on the FRET image (${}^{a}_{d}F$), which is usually the noisiest of the dataset. To enhance the quality of this image, the brightness of the red fluorophore can be improved by optimizing two experimental parameters: the quantum yield and the detection efficiency. In the present case, the detection in the red is not optimum due to the PMT detectors. CCD-based or avalanche photodiode-based detection have better quantum efficiencies and would improve the sensitivity in the red part of the spectrum. TMR is an excellent red fluorophore with a quantum yield close to unity. Unfortunately, it was slightly quenched by the DNA, which decreased its quantum yield to 0.63. This is still a respectable quantum yield for a red fluorophore. It is, for instance, four times larger than the quantum yield of Cy3 often used to tag antibodies in FRET experiments, and is comparable to DsRed (0.79) but still much larger than mRFP1 0.25.[10]

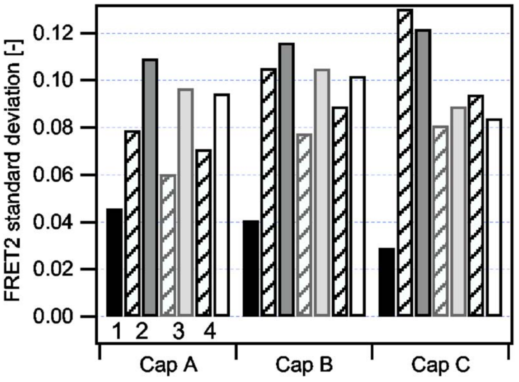

Fig. 6 Standard deviation of the FRET 2 index in each capillary as a function of the data analysis algorithm: 1. global fitting of FLIM data, 2. two-channel algorithm, 3. spectral imaging with spectral decomposition, and 4. spectral imaging split for two-channel algorithm. The dashed bars correspond to the calculated FRET2 error based on Poisson statistics for the intensity measurements.

The noise in all the images is directly linked to the number of photons collected. Therefore, the signal collected by the detector must be maximized. In two-channel imaging, spectral bleed-through is often eliminated by choosing narrow spectral windows, but this often results in increased photon loss. One should, on the contrary, try to maximize the fluorescence collected and rely on the Gordon's algorithm to efficiently account for the bleed-through. Spectral imaging is the natural extension of this observation, because all the emitted fluorescence is collected without any light losses due to filters and beamsplitters. However, our setup suffers from other losses that are present in the spectral imaging path. Thus, the measured green intensities in the green channel or in the green part of the spectrum are relatively similar.

The difference between the two types of data analysis of the spectral images is minor. In capillary A, the green emission dominates the spectrum and the TMR emission appears only as a shoulder on the Oregon Green emission. Resolving precisely the contribution of the red fluorophore with spectral decomposition is hard under those conditions. In capillary C, where the two fluorophores are contributing more equally to the emission, the spectral decomposition performs more efficiently and the measured standard deviation is better than the one obtained from a simple split in green and red contributions. In cases where the two dyes have closer emission spectra, or if a third species (autofluorescence) is present in the image, it might also be more advantageous to use the spectral decomposition technique. Thaler et al. have developed an elegant technique that couples the spectral decomposition of the image set directly with the calculation of the FRET efficiency based on linear unmixing.[32]

The FLIM clearly delivers errors two to three times smaller than the measured standard deviation obtained with other techniques. The advantage of this modality is that it relies only on the measurement of the donor image $({}^{d}_{d}F)$, which is the brightest image of the dataset. FLIM can even be used to monitor the energy transfer process toward nonfluorescing acceptors.

The other main advantage of lifetime imaging is that the proportion of interacting versus free donors in the image can be extracted using a global fitting algorithm. From the two lifetimes of the image, the distance separating the two dyes (50 Å) can be calculated, which is close to the expected distance discussed previously (Table 3). For capillaries A and D, where a ratio of zero is expected, there is an offset due to the fitting of a double exponential decay to noisy decay curves, which results in an overestimation of the contribution of the faster decay component. This artifact was already observed in other global fitting analyses.[34] For the other capillaries, the ratio, increases linearly with the expected ratio, with an error in the determination of the interacting ratio on the order of 10%. This can be improved by lengthening the acquisition time and thus improving the signal-to-noise ratio. Additionally, one could implement a global fitting algorithm that also takes into account the fluorescence decay of the acceptor. This might improve the resolution of the FRET lifetime and thus the characterization of the interaction ratio.

One often mentioned criticism addressed to FLIM imaging is the fact that the image acquisition is slow.[32] Acquiring an image with enough photons detected in each pixel to build a good lifetime histogram can take up to five to ten minutes, depending on the sample. A bright sample delivers 10^6 photons/sec. In 5 min, one counts roughly 4500 photons per pixel in a 256×256 image, which is more than enough to use in a global fitting routine.

The acquisition time is directly linked to the dye concentration in the sample and the excitation intensity: the larger the emitted photon flux, the shorter the imaging time. This holds true until one reaches saturation of the detector. Due to the time correlation electronics, saturation is reached at lower light levels for the FLIM acquisition than for intensity-based detection, where it is even possible to work in dc mode instead of photon counting mode to accommodate the highest intensity levels. However, in common FRET experiments where FP constructs are artificially produced by cells, it is important not to overexpress these proteins to retain physiologically relevant concentration levels. Moreover, excitation energies are also kept low to avoid photobleaching and other unwanted side effects. Therefore, typical fluorescence photon fluxes in those experiments are well within the range where TCSPC are operational. Within this range, we have shown that they provide the most accurate way to quantify FRET.

6 Conclusion

Using a doubly labeled DNA strand, it is possible to generate a FRET construct with a fixed efficiency. For a separation of ten base pairs between Oregon Green 488 (the donor) and tetramethylrhodamine (the acceptor), an efficiency of 80% is obtained. This construct is used in a real imaging situation using an image formed by microcapillaries containing different ratios of the FRET construct and non-FRETting DNA strands. Four different analysis methods are used. The first uses a two-channel detection scheme based on Gordon's algorithm, which allows the FRET2 index to be calculated and a measure of the amount of FRET occurring in each pixel of the image. The distribution of the FRET2 values are found to be mainly governed by Poisson noise, thus an increase in accuracy would require a longer acquisition time or a higher photon flux. The second imaging modality used is spectral imaging, where two different analysis methods are employed. Both yield slightly improved distribution than the simple two-channel measurements. The spectral decomposition optimization employed could prove very powerful in systems with larger spectral overlap. Further technical improvements could also help this type of analysis by improving the detection efficiency in the red part of the spectrum. Finally, the FLIM images provide the best assessment of the FRET2 index. Based on a global fitting algorithm, this analysis also delivers significantly smaller uncertainty on the FRET2 index than other methods. Since the detection and quantification of protein-protein interactions in cells are often limited by experiment precision, lifetime approach should be considered in certain cases despite the inherent instrument complexity. Further, the FLIM approach also allows the ratio of FRET construct over total green dye in each pixel of the image to be measured, allowing the quantification of the fraction of interacting proteins in cells.

Acknowledgment

This work has been supported by the National Institute of Health grant NIHPOIHL64858.

References

1. B. S. Gaylord, M. R. Massie, S. C. Feinstein, and G. C. Bazan, "SNP detection using peptide nucleic acid probes and conjugated polymers: applications in neurodegenerative disease identification," *Proc. Natl. Acad. Sci. U.S.A.* **102**(1), 34–39 (2005).
2. D. J. Lichlyter, S. A. Grant, and O. Soykan, "Development of a novel FRET immunosensor technique," *Biosens. Bioelectron.* **19**(3), 219–226 (2003).
3. H. J. Youn, E. Terpetschnig, H. Szmacinski, and J. R. Lakowicz, "Fluorescence energy transfer immunoassay based on a long-lifetime luminescent metal-ligand complex," *Anal. Biochem.* **232**(1), 24–30 (1995).
4. X. Zhuang and M. Rief, "Single-molecule folding," *Curr. Opin. Struct. Biol.* **13**(1), 88–97 (2003).
5. S. Weiss, "Measuring conformational dynamics of biomolecules by single molecule fluorescence spectroscopy," *Nat. Struct. Biol.* **7**(9), 724–729 (2000).
6. E. A. Jares-Erijman and T. M. Jovin, "FRET imaging," *Nat. Biotechnol.* **21**(11), 1387–1395 (2003).
7. A. K. Kenworthy, "Imaging protein-protein interactions using fluorescence resonance energy transfer microscopy," *Methods* **24**(3), 289–296 (2001).
8. R. B. Sekar and A. Periasamy, "Fluorescence resonance energy transfer (FRET) microscopy imaging of live cell protein localizations," *J. Cell Biol.* **160**, 629–633 (2003).
9. J. D. Mills, J. R. Stone, D. G. Rubin, D. E. Melon, D. O. Okonkow, A. Periasamy, and G. A. Helm, "Illuminating protein interactions in tissue using confocal and two-photon excitation fluorescence resonance energy transfer microscopy," *J. Biomed. Opt.* **8**(3), 347–356 (2003).

10. R. E. Campbell, O. Tour, A. E. Palmer, P. A. Steinbach, G. S. Baird, D. A. Zacharias, and R. Y. Tsien, "A monomeric red fluorescent protein," *Proc. Natl. Acad. Sci. U.S.A.* **99**(12), 7877–7882 (2002).
11. G. S. Baird, D. A. Zacharias, and R. Y. Tsien, "Biochemistry, mutagenesis, and oligomerization of DsRed, a red fluorescent protein from coral," *Proc. Natl. Acad. Sci. U.S.A.* **97**(22), 11984–11989 (2000).
12. R. Y. Tsien, "The green fluorescent protein," *Annu. Rev. Biochem.* **67**, 509–544 (1998).
13. M. Zimmer, "Green fluorescent protein (GFP): Applications, structure, and related photophysical behavior," *Chem. Rev. (Washington, D.C.)* **102**, 759–781 (2002).
14. M. Tramier, I. Gautier, T. Piolot, S. Ravalet, K. Kemnitz, J. Coppey, C. Durieux, V. Mignotte, and M. Coppey-Moisan, "Picosecond-hetero-FRET microscopy to probe protein-protein interactions in live cells," *Biophys. J.* **83**(6), 3570–3577 (2002).
15. T. Kohl, K. G. Heinze, R. Kuhlemann, A. Koltermann, and P. Schwille, "A protease assay for two-photon crosscorrelation and FRET based solely on fluorescent proteins," *Proc. Natl. Acad. Sci. U.S.A.* **99**(19), 12161–12166 (2002).
16. D. R. Larson, Y. M. Ma, V. M. Vogt, and W. W. Webb, "Direct measurement of Gag-gag interaction during retrovirus assembly with FRET and fluorescence correlation spectroscopy," *J. Cell Biol.* **162**, 1233–1244 (2003).
17. L. Tremuth, S. Kreis, C. Melchior, J. Hoebeke, P. Ronde, S. Plancon, K. Takeda, and N. Kieffer, "A fluorescence cell biology approach to map the second integrin-binding site of talin to a 130-amino acid sequence within the rod domain," *J. Biol. Chem.* **279**(21), 22258–22266 (2004).
18. G. W. Gordon, G. Berry, X. H. Liang, B. Levine, and B. Herman, "Quantitative fluorescence resonance energy transfer measurements using fluorescence microscopy," *Biophys. J.* **74**, 2702–2713 (1998).
19. C. Berney and G. Danuser, "FRET or no FRET: A quantitative study," *Biophys. J.* **84**, 3992–4010 (2003).
20. M. Elangovan, H. Wallrabe, Y. Chen, R. N. Day, M. Barroso, and A. Periasamy, "Characterization of one- and two-photon excitation fluorescence resonance energy transfer microscopy," *Methods* **29**(1), 58–73 (2003).
21. A. Hoppe, K. Christensen, and J. A. Swanson, "Fluorescence resonance energy transfer-based stoichiometry in living cells," *Biophys. J.* **83**, 3652–3664 (2002).
22. Z. Xia and Y. Liu, "Reliable and global measurement of fluorescence resonance energy transfer using fluorescence microscopes," *Biophys. J.* **81**, 2395–2402 (2001).
23. N. Mochizuki, S. Yamashita, K. Kurokawa, Y. Ohba, T. Nagai, A. Miyawaki, and M. Matsuda, "Spatio-temporal images of growth-factor-induced activation of Ras and Rap1," *Nature (London)* **411**(6841), 1065–1068 (2001).
24. M. Elangovan, R. N. Day, and A. Periasamy, "Nanosecond fluorescence resonance energy transfer-fluorescence lifetime imaging microscopy to localize the protein interactions in a single living cell," *J. Microsc.* **205**, 3–14 (2002).
25. P. J. Verveer, F. S. Wouters, A. R. Reynolds, and P. I. H. Bastiaens, "Quantitative imaging of lateral ErbB1 receptor signal propagation in the plasma membrane," *Science* **290**, 1567–1570 (2000).
26. B. J. Bascskai, J. Skoch, G. A. Hickey, R. Allen, and B. T. Hyman, "Fluorescence resonance energy transfer determinations using multiphoton fluorescence lifetime imaging microscopy to characterize amyloid-beta plaques," *J. Biomed. Opt.* **8**(3), 368–375 (2003).
27. Y. Chen and A. Periasamy, "Characterization of two-photon excitation fluorescence lifetime imaging microscopy for protein localization," *Microsc. Res. Tech.* **63**, 72–80 (2004).
28. L. Stryer and R. P. Haugland, "Energy transfer: a spectroscopic ruler," *Proc. Natl. Acad. Sci. U.S.A.* **58**, 719–726 (1967).
29. P. Wu and L. Brand, "Resonance energy transfer: methods and applications," *Anal. Biochem.* **218**(1), 1–13 (1994).
30. G. H. Patterson, D. W. Piston, and B. G. Barisas, "Förster distances between green fluorescent protein pairs," *Anal. Biochem.* **284**, 438–440 (2000).
31. W. R. Zipfel, R. M. Williams, R. Christie, A. Y. Nikitin, B. T. Hyman, and W. W. Webb, "Live tissue intrinsic emission microscopy using multiphoton-excited native fluorescence and second harmonic generation," *Proc. Natl. Acad. Sci. U.S.A.* **100**(12), 7075–7080 (2003).
32. C. Thaler, S. V. Koushik, P. S. Blank, and S. S. Voge, "Quantitative multiphoton spectral imaging and its use for measuring resonance energy transfer," *Biophys. J.* **89**(4), 2736–2749 (2005).
33. T. Haraguchi, T. Shimi, T. Koujin, N. Hashiguchi, and Y. Hiraoka, "Spectral imaging fluorescent microscopy," *Genes Cells* **7**, 881–887 (2002).
34. S. Pelet, M. J. Previte, L. H. Laiho, and P. T. So, "A fast global fitting algorithm for fluorescence lifetime imaging microscopy based on image segmentation," *Biophys. J.* **87**(4), 2807–2817 (2004).
35. P. J. Verveer, A. Squire, and P. I. H. Bastiaens, "Global analysis of fluorescence lifetime imaging microscopy data," *Biophys. J.* **78**, 2127–2137 (2000).
36. C. Buehler, K. H. Kim, U. Greuter, N. Schlumpf, and P. T. So, "Single-photon counting multicolor multiphoton fluorescence microscope," *J. Fluoresc.* **15**(1), 41–51 (2005).
37. E. Rusinova, V. Tretyachenko-Ladokhina, O. E. Vele, D. F. Senear, and J. B. Alexander Ross, "Alexa and Oregon Green dyes as fluorescence anisotropy probes for measuring protein-protein and protein-nucleic acid interactions," *Anal. Biochem.* **308**(1), 18–25 (2002).
38. J. R. Unruh, G. Gokulrangan, G. S. Wilson, and C. K. Johnson, "Fluorescence properties of fluorescein, tetramethylrhodamine, and Texas Red linked to a DNA aptamer," *Photochem. Photobiol.* **81**(3), 682–690 (2005).
39. A. A. Deniz, M. Dahan, J. R. Grunwell, T. Ha, A. E. Faulhaber, D. S. Chemla, S. Weiss, and P. G. Schultz, "Single-pair fluorescence resonance energy transfer on freely diffusing molecules: observation of Forster distance dependence and subpopulations," *Proc. Natl. Acad. Sci. U.S.A.* **96**, 3670–3675 (1999).
40. R. M. Clegg, "Fluorescence resonance energy transfer and nucleic acids," *Methods Enzymol.* **211**, 353–388 (1992).
41. R. M. Clegg, "Observing the helical geometry of double-stranded DNA in solution by fluorescence resonance energy transfer," *Proc. Natl. Acad. Sci. U.S.A.* **90**, 2994–2998 (1993).
42. K. M. Parkhurst and L. J. Parkhurst, "Donor-acceptor distance distribution in a double-labeled fluorescent oligonucleotide both as a single strand and in duplexes," *Biochemistry* **34**, 293–300 (1995).
43. K. Toth, V. Sauermann, and J. Langowski, "DNA curvature in solution measured by fluorescence resonance energy transfer," *Biochemistry* **37**, 8173–8179 (1998).
44. G. M. Bonamy, A. Guiochon-Mantel, and L. A. Allison, "Cancer promoted by the oncoprotein v-ErbA may be due to subcellular mislocalization of nuclear receptors," *J. Mol. Endocrinol.* **19**(5), 1213–1230 (2005).